Int. J. Electrochem. Sci., 12 **(2017)** 3686 – 3696, doi: 10.20964/2017.05.36

International Journal of
ELECTROCHEMICAL
SCIENCE
www.electrochemsci.org

Electrode Behaviors of $BiFeO_3$ Powders: A Possible Application of Bi_2O_3 Oxide in Rechargeable Battery

Pengfei Yuan, Huaiying Zhou [*], *Zhongmin Wang* [*], *Jianqiu Deng, Peng Liu ,Qingrong Yao*

School of Material Science and Engineering, Guilin University of Electronic Technology, Guangxi, Guilin 541004, China
[*]E-mail: zhy@guet.edu.cn, zmwang@guet.edu.cn

Received: 6 December 2016 / *Accepted:* 11 March 2017 / *Published:* 12 April 2017

Pure phase $BiFeO_3$ nanopowders were successfully prepared by a sol-gel method. The phase structure and morphology were characterized by XRD and SEM analysis technique. For the first time, the electrochemical properties of $BiFeO_3$ nanopowders were evaluated as anode materials for the alkaline secondary batteries. The results indicate that as-prepared $BiFeO_3$ oxides are perovskite-type nanopowders with high crystallinity. As negative electrode in $Ni(OH)_2$ / $BiFeO_3$ battery, the $BiFeO_3$ oxides irreversibly decompose into Bi_2O_3 and Fe_2O_3 in the initial charge-discharge cycling., In subsequent cycles, both of Bi_2O_3 and Fe_2O_3 oxides act as effective electrode materials in designed battery system. The pure Bi_2O_3 shows the best performance by comparing the electrochemical properties among $BiFeO_3$, Bi_2O_3 and Fe_2O_3. The maximum discharge capacity of Bi_2O_3 electrodes is 285 mAh/g, and the capacity retention after 20 charge-discharge cycles is 87%, indicating that it is a promising electrode material in alkaline rechargeable battery.

Keywords: Perovskite-type oxide, $BiFeO_3$, Bi_2O_3, Decomposition, Electrode properties.

1. INTRODUCTION

Nickel/metal hydride (Ni/MH) secondary batteries have been widely employed in portable electrical devices and power sources due to their high performance [1-5]. But in recent years, Ni/MH battery is encountering serious competition from Li-ion batteries [6-8] and other advanced secondary batteries, it is more urgent to reduce production cost and improve the capacity and cycle life of Ni/MH batteries to enhance their competition in the rechargeable battery market.

In order to raise the competitiveness of Ni/MH batteries, some attempts have been done. Esaka et al. [9] have firstly proposed perovskite-type oxides $ACe_{1-x}M_xO_{3-\delta}$ (A = Sr or Ba, M = rare earth

element) prepared by a conventional solid-state reaction method as electrode materials for Ni/MH batteries. Its electrochemical hydrogen storage mechanism is:

$$BaCe(IV)_{0.95}\,Nd_{0.05}O_{3-\delta} + x\,H_2O + xe^- \underset{discharge}{\overset{charge}{\rightleftharpoons}} BaCe(IV)_{0.95-x}\,Ce(III)_x\,Nd_{0.05}O_{3-\delta}H(I)_x + x\,OH^-$$

However, its maximum discharge capacity is only 119 mAh/g at the current density of 9.25 mA/g. Lim et al. [10] have reported that the discharge capacity of the ABO_3-type perovskite oxide $LaCoO_3$ is 42.4 mAh/g at a discharge current density of 20 mA/g under the temperature of 298 *K*.

The perovskite-type bismuth orthoferrite ($BiFeO_3$) is of great interest because of its high potential for advanced technologies. $BiFeO_3$ has been investigated for application as capacitors, nonvolatile memory, and magnetoelectric devices [11–14]. Photocatalytic activities of $BiFeO_3$ have also been reported [15, 16]. In the recent works, Gao et al. [17] have found that the application of $BiFeO_3$ for electrode material of lithium battery and its first discharge capacity is about 1000 mAh/g. Lu et al. [18] have prepared $BiFeO_3$ thin film and it is tested as anode material in lithium-ion batteries whose reversible capacity about 770 mAh / g and about 50% of its initial reversible capacity can be maintained after 50 cycles. Since $BiFeO_3$ is also perovskite–-type ABO_3 oxide, how about its application in Ni/MH battery?

In this paper, $BiFeO_3$ nanopowders have been prepared by a sol-gel method, the electrode properties of $BiFeO_3$ as negative electrode in $Ni(OH)_2/BiFeO_3$ battery system have been investigated by a simulated battery. Especially, its hydrogen storage mechanism and structure evolution during the charge-discharge process have been firstly discussed in alkaline solution.

2. EXPERIMENTAL

2.1 Preparation of $BiFeO_3$ nanopowders

All the raw materials were purchased from Xilong Chemical Co., Ltd, including Bismuth nitrate pentahydrate ($Bi(NO_3)_3{\cdot}5H_2O$), Iron nitrate nonahydrate ($Fe(NO_3)_3{\cdot}9H_2O$), acetic acid and soluble starch. All of the chemicals were of analytical grade and as received without further purification.

$BiFeO_3$ oxide powders were synthesized via a sol-gel method [19]. In this work, 0.006 mol $Bi(NO_3)_3{\cdot}5H_2O$ and $Fe(NO_3)_3{\cdot}9H_2O$ were dissolved in a solution contained 2 g acetic acid and 8 ml deionized water to obtain a brown and transparent mixture solution under stirring. Then 6 g soluble starch was slowly added to the mixed solution. The mixed solution turned into a high viscous gel under continuous stirring for 5 h at a gently temperature (70 ^oC) to remove the excess water. Subsequently, the $BiFeO_3$ nanopowders were obtained by sintering at 600 ^oC for 1 h in air. For comparison, the Bi2O3 and Fe2O3 nanopowders were also synthesized by the same method.

2.2 Structural characterization

The crystal structure of the as-prepared $BiFeO_3$ oxide powders was determined by powder X-ray diffraction (XRD, PANalytical X'pert PRO high resolution diffractometer,) using Cu Kα radiation.

The diffraction data were collected from 20° to 80° at a scan rate of 2°/min, then analyzed and refined with Full-prof program. The scanning electron microscopic (SEM) images of these powders were collected using a FEI 450scanning electron microscope.

2.3 Electrochemical measurements

The electrochemical properties of $BiFeO_3$ nanopowders were evaluated using a simulated cell. The negative electrodes were prepared by cold pressing the mixture of 0.1 g $BiFeO_3$ powders and 0.4 g nickel powders under 10 MPa to form pellets of 15 mm in diameter. Here the commercial nickel hydroxide ($Ni(OH)_2$) was used as the counter electrode (positive)， the negative electrode was sandwiched between two positive electrodes, and the electrolyte was 6 M KOH solution.

Charge-discharge tests were carried out on an Arbin BT-2000 battery testing instrument. In the charge-discharge testing, the electrodes were fully charged for 7 h at current density of 50 mA/g, and then discharged at the same current density to a cut-off potential of 0.6 *V*. The cyclic voltammetry (CV) curve was recorded by scanning electrode potential at the rate 0.1 mV/s from -0.2 to -1.2 V (vs. Hg/HgO) through a Modulab (Solartron Analytical) electrochemical workstation.

3. RESULTS AND DISCUSSION

3.1 Characterization of as-prepared $BiFeO_3$ powders

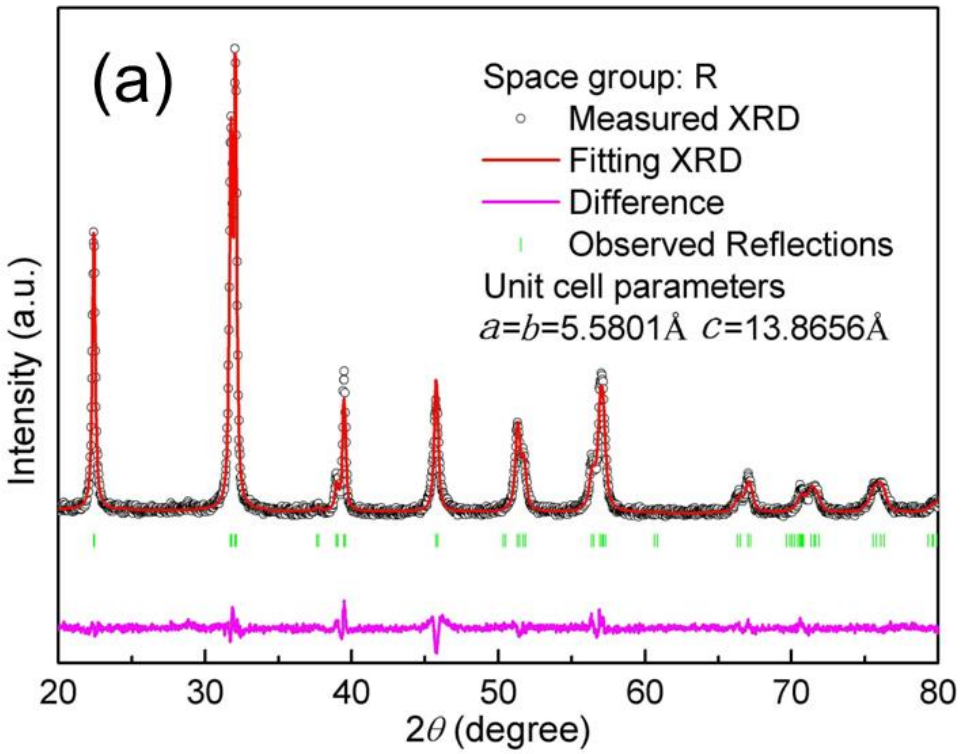

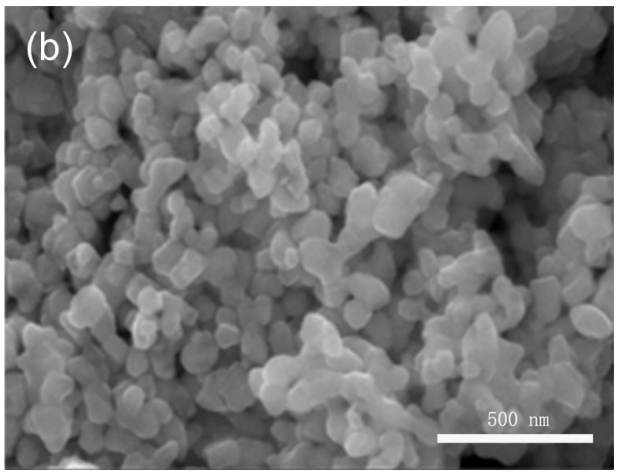

Figure 1. (a) XRD pattern and Rietveld refinement of the perovskite-type $BiFeO_3$ nanopowders, (b) SEM image of $BiFeO_3$.

The XRD pattern of as-prepared $BiFeO_3$ nanopowders is shown in Fig. 1a. From the XRD pattern, $BiFeO_3$ nanopowders show a high degree of crystallinity. Rietveld refinement on the XRD pattern was performed using the Full-prof programs to analyze the crystal structure of $BiFeO_3$ phase. The refined result is also displayed in Fig. 1a. The refined and observed patterns match well. The reliability factor is good (R_w = 1.19). $BiFeO_3$ is indexed as rhombohedral unit cell with the R space group (ICSD no.20-0169) sans impurities. The refined unit cell parametersof $BiFeO_3$ are a=5.5801 Å and c=13.8656 Å, which are in good agreement with the reported results from Ashwini Kumar [20] and Eva Gil-González [21]. Fig. 1b depicts the SEM images of as-prepared $BiFeO_3$ powders. The sample shows irregular particles with small agglomerates. The average particle size is about 97 nm measured with Nano Measurer 1.2 programs.

3.2 Electrode properties of $BiFeO_3$ nanopowders in $Ni(OH)_2$/$BiFeO_3$ battery system

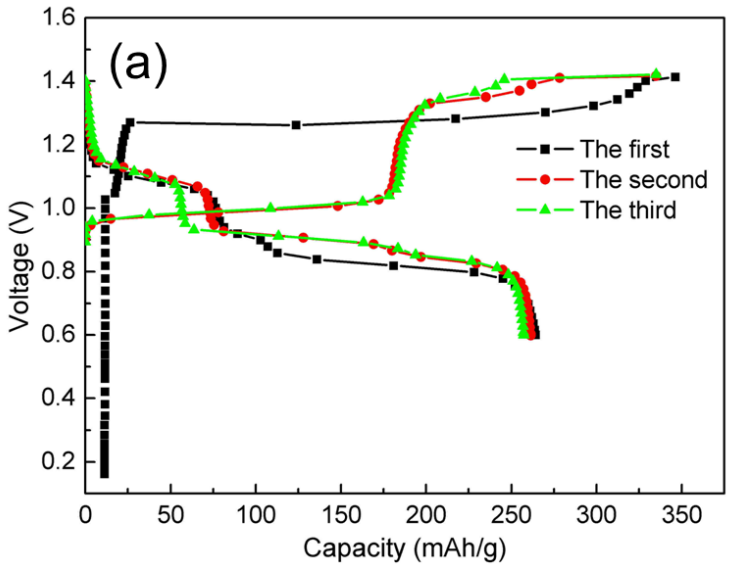

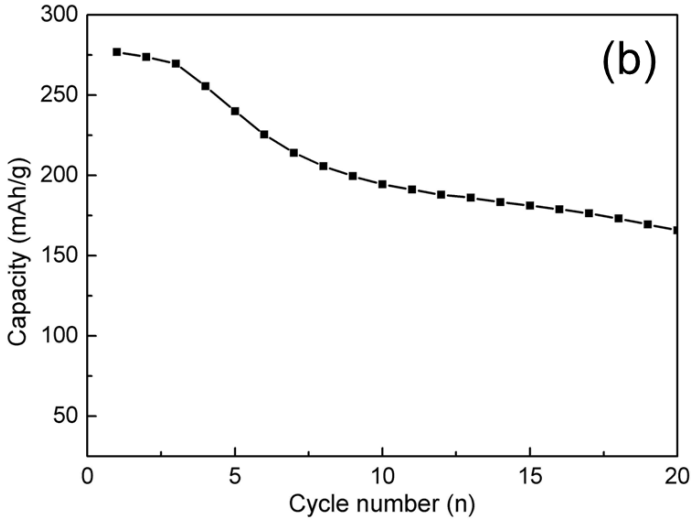

Figure 2. Electrochemical properties of $BiFeO_3$ electrodes at 50 mA/g: (a) charge/discharge curves, (b) cycling stability.

The electrochemical properties of $BiFeO_3$ electrodes are evaluated by the charge-discharge testing at a current density of 50 mA/g. The first three charge/discharge curves of the $BiFeO_3$ electrodes are presented in Fig. 2a. It can be clearly seen that there are two potential plateaus at the charge/discharge curves. For the first cycle, the only one charge plateau is found at about 1.25 V and the two discharge plateaus are about 1.1 V and 0.8 V, respectively. However, there are two charge plateaus in subsequent charge-discharge cycles, which are located at around 1.0 V and 1.3 V. The discharge plateaus are similar in cycling, locating at 1.1 V and 0.9 V, respectively. The difference of charge plateau of $BiFeO_3$ electrodes during cycling will be detailedly discussed in next section of this paper. The cycling performance of $BiFeO_3$ electrodes is shown in Fig.2a. The maximum discharge capacity of 264 mAh/g is obtained in the first charge-discharge cycle, which is about twice that reported in previous works [22-24]. But an obvious decrease of capacity is observed in the subsequent cycles. The discharge capacity retention ratio is only 63% after 20 cycles at the room temperature, indicating a poor cycling stability of $BiFeO_3$ electrodes. The reasons of rapid capacity fading will also investigated below.

To explain the difference of charge plateaus and reasons of rapid capacity fading on the $BiFeO_3$ electrodes, the ex-situ XRD analysis and CV measurements were performed during the charge-discharge testing of $BiFeO_3$ electrodes. For ex-situ XRD analysis, the electrodes at different state of charge/discharge were broken off, washed with distilled water and absolute ethanol for three times, and dried under vacuum at 50 ^oC for 12 h, then cooled to room temperature. The ex-situ XRD patterns of $BiFeO_3$ electrodes at various state of charge/discharge during the initial charge-discharge testing are displayed in Fig. 3. It is noted that $BiFeO_3$ decomposes gradually into Fe_2O_3 and Bi_2O_3 during the initial charging process, and then Fe_2O_3 and Bi_2O_3 acts as the active materials for the electrode reaction during the charge process. $BiFeO_3$ is completely decomposed into Fe_2O_3 and Bi_2O_3 at the end of charging. The resulted Bi_2O_3 decomposes into Bi and Fe_2O_3 transforms into $Fe(OH)_2$. From Fig.3, there are only two phases Fe_2O_3 and Bi_2O_3 after fully discharging, implying the Bi and $Fe(OH)_2$ turn

into Bi_2O_3 and Fe_2O_3, respectively, in the discharge process. The reactions of Bi_2O_3 and Fe_2O_3 electrodes in alkaline aqueous electrolyte have been reported in the literatures [25-30]. The phase transformation of electrode materials explains the difference of charge plateaus during the charge-discharge process.

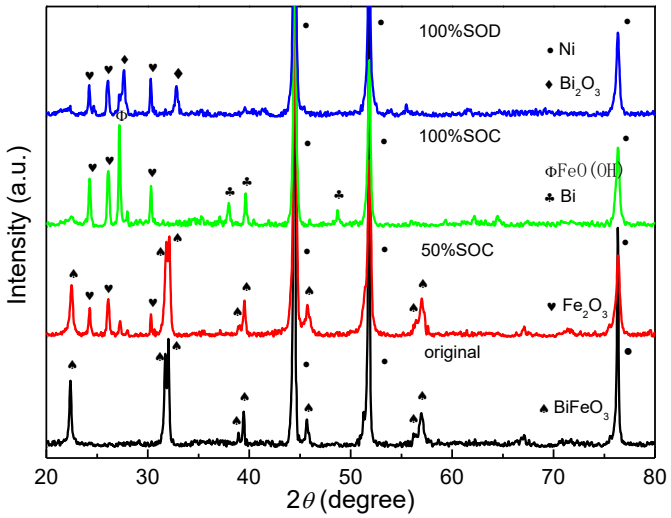

Figure 3. XRD patterns of the $BiFeO_3$ electrodes at various states of charge/discharge.

The CV curves of $BiFeO_3$, Fe_2O_3/Bi_2O_3, Bi_2O_3 and Fe_2O_3 electrodes were obtained, as shown in Fig. 4, to confirm the decomposition of $BiFeO_3$ during the charging and further analyze the electrode properties of the oxides. The Fe_2O_3/Bi_2O_3 mixture electrodes were prepared according to the mass ratio of Fe_2O_3:Bi_2O_3=1:1. For the $BiFeO_3$ electrodes, the two pairs of redox peaks are around -0.6/-0.9 V and -0.35/-0.6 V in the first CV curve, while the redox peaks are located at about -0.65/-0.95 V and -0.4/-0.65 V, respectively, in the subsequent cycles.

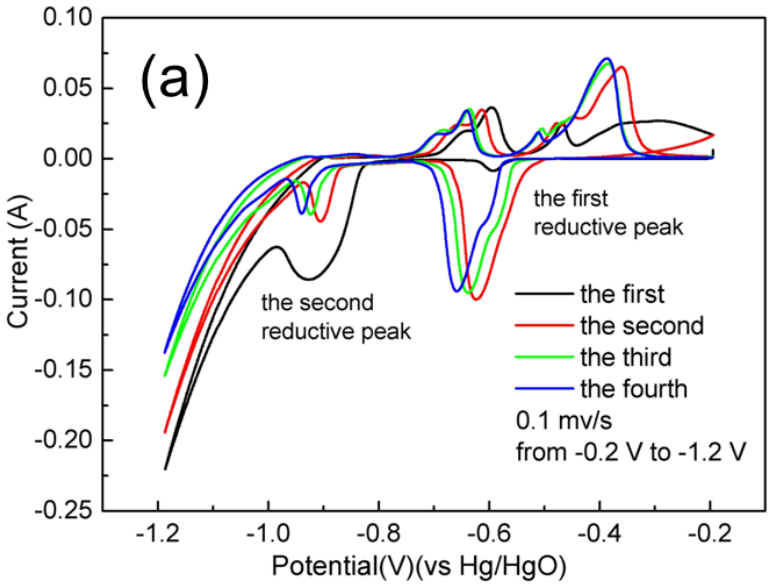

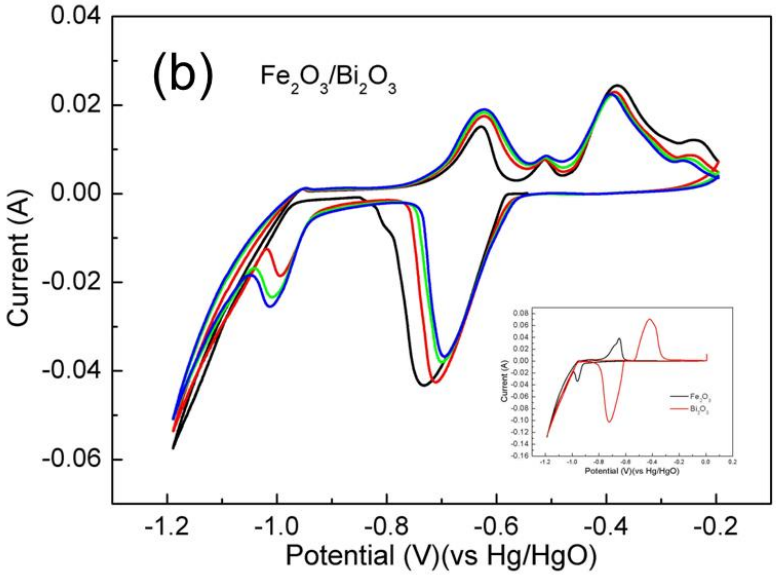

Figure 4. Typical CV curves of the electrodes at the rate 0.1 mV/s from -0.2 to -1.2 V (vs. Hg/HgO) in a 6 *M* KOH solution: (a) $BiFeO_3$ electrode, (b) Fe_2O_3/Bi_2O_3 electrodes. The inset in Fig.4b is the CV curves of Fe_2O_3 and Bi_2O_3 electrodes.

The two pairs of reduction peaks on each cycle indicate that two step redox reactions exist during the charge/discharge process. From Fig.4b, we can find the redox peaks position of Fe_2O_3/Bi_2O_3 mixture electrodes is in good agreement with the second CV curves of $BiFeO_3$ electrodes. This result confirms that $BiFeO_3$ decomposes into Fe_2O_3 and Bi_2O_3 in the first charge cycling. Compared with the CV curves of Fe_2O_3 and Bi_2O_3 electrodes, the redox peaks at 0.4/0.65 V represents the Bi/Bi_2O_3 redox reaction, the pair of redox peaks located at -0.65/-0.95 V correspond to Fe/Fe_2O_3 oxidation/reduction reaction. The first redox peaks at -0.35/-0.6 V are much smaller than the subsequent cycles, due to fast decomposition of $BiFeO_3$ and the instantaneous transformation of Bi_2O_3 into Bi. The decreasing redox peaks of Fe_2O_3 during cycling could be ascribed to the low conductivity of the formed $Fe(OH)_2$, hindering the charged species transport [25]. Based on CV and ex-situ XRD analysis, the electrode reaction of $BiFeO_3$ can be deduced as the following [25-38]: (1) $BiFeO_3$ irreversibly decomposes into Fe_2O_3 and Bi_2O_3 during the charge process. (see equation a). (2) The reversible redox reaction between the formed Fe_2O_3 and $Fe(OH)_2$ represents by equation b. (3) The reversible oxidation/reduction reaction exists in Bi_2O_3 and Bi, see equation c.

$$2BiFeO_3 \xrightarrow{\text{charge}} Bi_2O_3 + Fe_2O_3 \qquad \text{(a)}$$

$$Fe_2O_3 + 3H_2O + 2e^- \xleftrightarrow{\text{chrge/discharge}} 2Fe(OH)_2 + 2OH^- \qquad \text{(b)}$$

$$Bi_2O_3 + 3H_2O + 6e^- \xleftrightarrow{\text{charge/discharge}} 2Bi + 6OH^- \qquad \text{(c)}$$

In order to further investigate the reasons of rapid capacity fading on the $BiFeO_3$ electrodes and explore the electrode properties of Bi_2O_3 electrodes, the electrochemical performance of Fe_2O_3, Bi_2O_3 and Fe_2O_3/Bi_2O_3 electrodes were evaluated by the charge-discharge testing at a current density of 50

mA/g. The first three charge/discharge curves are shown in Fig. 5a. For Fe_2O_3 and Bi_2O_3 electrodes, the charge/discharge plateaus are about 1.35/1.2 V and 1.0/0.9 V, respectively, which is consistent with the previously reported results [39, 40]. For Fe_2O_3/Bi_2O_3 electrodes, there are two potential plateaus located at about 1.35 /1.05 V and 1.1/0.9 V during charge-discharge cycling, similar to the $BiFeO_3$ electrodes. So we could conclude that the discharge capacity of $BiFeO_3$ at 1.1 V is mainly related to Fe_2O_3, and the discharge capacity at 0.9 V is associated with Bi_2O_3.

Fig. 5b presents the discharge capacity of the three electrodes. The maximum discharge capacity is 107 mAh/g and 285 mAh/g for Fe_2O_3 and Bi_2O_3 electrodes, and the capacity retention after 20 charge/discharge cycles are 46% and 87%, respectively. Similar to $BiFeO_3$ electrodes, Fe_2O_3/Bi_2O_3 electrodes deliver a relative high maximum discharge capacity (226 mAh/g) and rapid capacity fading.

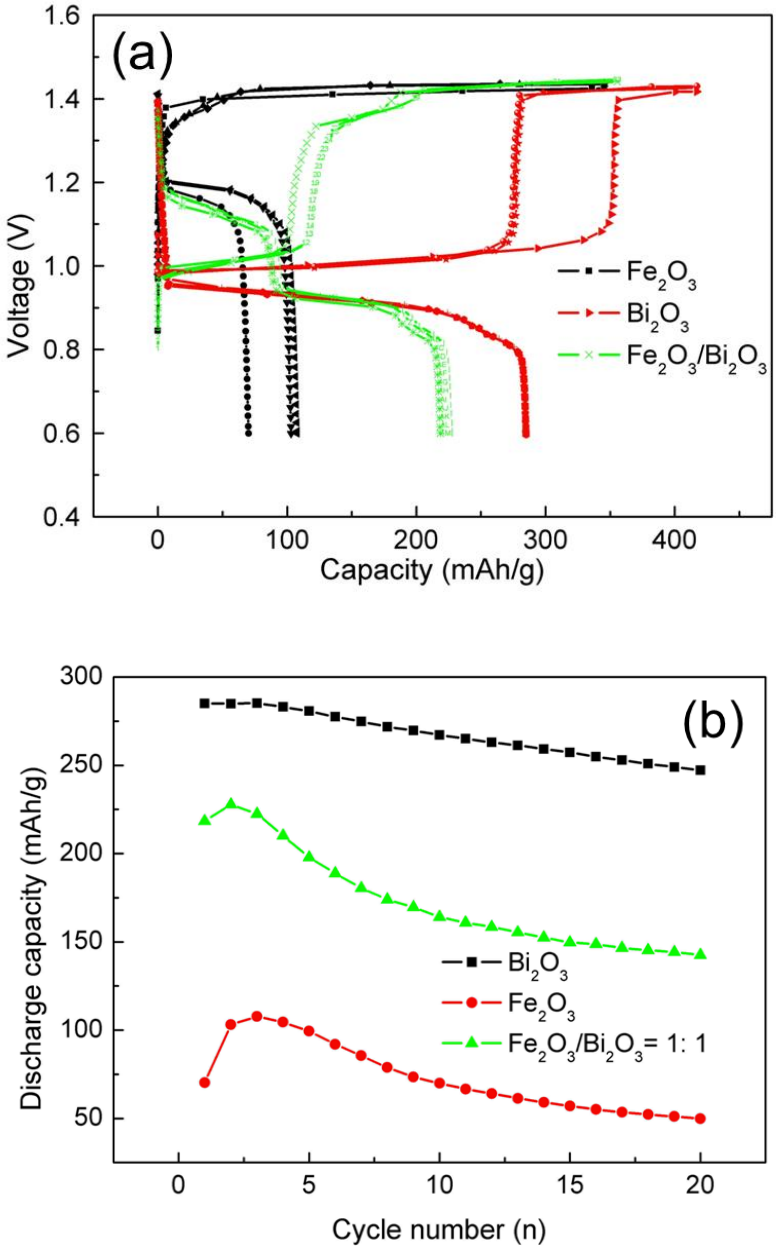

Figure 5. The electrode properties of Fe_2O_3, Bi_2O_3 and Fe_2O_3/Bi_2O_3 electrodes at 50 mA/g: (a) the first three charge/discharge curves, (b) cycling stability.

Although the discharge plateaus of Bi_2O_3 electrodes is lower than that of traditional hydrogen storage alloy electrodes [41-44], it can be interpreted from the following several aspects, first, iron electrode is easy to corrosion in alkaline solution, because the steady potential of the iron in alkaline solution smaller than hydrogen balance potential 40~50 mV, and hydrogen and separation overpotential of hydrogen is small on the iron electrode, at the same time, oxygen ionization potential is not big [45]; second, adsorption of oxygen electrode surface will cause the passivation of iron, a monolayer adsorption oxygen could make the iron electrode passivation completely, stop the electronic exchange reaction [46-48]; third, the structure of the electrode material is too dense that make effective electrode surface area is too small [48], it is worth further study for its suitable capacity and good cycle stability. The rapid capacity fading on the $BiFeO_3$ electrodes could be ascribed to the formation of Fe_2O_3. The formed Fe_2O_3 acts as the active material in the electrodes, resulting the low capacity and fast capacity fading.

4. CONCLUSIONS

Perovskite-type $BiFeO_3$ nanopowders with high degree of cystalinity and pure phase, have been prepared by a sol-gel method, using as anode materials for $Ni(OH)_2/BiFeO_3$ batteries in the alkaline solution. $BiFeO_3$ electrodes deliver a relative high maximum discharge capacity. The capacity fading, however, is relatively fast, due to the formation of Fe_2O_3 during the initial charge process. Through the investigation of the reasons of capacity fading on $BiFeO_3$ electrodes, we conclude that Bi_2O_3 electrodes demonstrate a high capacity and good cycling stability. The maximum discharge capacity of Bi_2O_3 electrodes is 285 mAh/g, and the capacity retention after 20 charge-discharge cycles is 87%. Although the relative low discharge plateaus of Bi_2O_3 electrode, it is worth further study for its good electrode properties.

ACKNOWLEDGEMENTS
This work was financially supported by the National Natural Science Foundation of China (No. 51471055, 51371061 and 21363005), Guangxi Experiment Center of Information Science, Guilin University of Electronic Technology (20130113) and the Guangxi Natural Science Foundation (2016GXNSFGA380001).

References

1. M. Raju, M.V. Ananth, L. Vijayaraghavan, *J. Power Sources*, 180 (2008) 830.
2. Y.F. Liu, H.G. Pan, M.X. Gao, Y.F. Zhu, Y.Q. Lei, Q.D. Wang, *Electrochim. Acta*, 49 (2004)545.
3. E.A. Kumar, M.P. Maiya, S.S. Murthy, B. Viswanathan, *J. Alloys Compd.*, 476 (2009) 92.
4. M. Tliha, C. Khaldi, H. Mathlouthi, J. Lamloumi, A. Percheron-Guegan, *J. Alloys Compd.*, 440 (2007) 323.
5. T. Sakai, H. Yoshinaga, H. Miyamura, N. Kuriyama, H. Ishikawa, *J. Alloys Compd.*, 180 (1992)37.
6. Y. Yang, Q. Sun, Y.S. Li, H. Li, Z.W. Fu, *J. Electrochem. Soc.*, 158 (2011) B 1211.

7. Y.C. Lu, Z. Xu, H.A. Gasteiger, S. Chen, K. Hamad-Schifferli, Y. Shao-Horn, *J. Am Chem. Soc*., 132 (2010) 12170.
8. T.H. Yoon, *J. Nanoscale Res Lett*, 7 (2012) 1.
9. T. Esaka, H. Sakaguchi, S. Kobayashi, *J. Solid-State Ionicsm*, 166 (2004) 351.
10. D.K. Lim, H.N. Im, J. Kim, S.J. Song, *J. Phys Chem Sol*,74 (2013) 115.
11. K.Y. Yun, M. Noda, M. Okuyama, *J. Phys Lett*, 83 (2003) 3981.
12. Y.H. Lee, J.M. Wu, C.H. Lai, *J. Phys Lett*, 88 (2006) 042903.
13. Y. Wei, X. Wang, J. Jia, X. Wang, *J. Ceram Int*, 38 (2012) 3499.
14. J.F. Scott, *J. Nat Mater*, 6 (2007) 256.
15. F. Gao, Y. Yuan, K.F. Wang, X.Y. Chen, F. Chen, J.M. Liu, Z.F. Ren, *J. Appl Phys Lett* , 89 (2006) 102506.
16. X. Wang, Y. Lin, X. Ding, J. Jiang, *J. Alloys Compd*, 509 (2011) 6585.
17. S.H. Luo, M. Gao, J. Chen, X.R. Xing, Z. Li, X.T. Zhou, W. Wen, *J. New Mater Electrochem Systl*, 14 (2011) 141.
18. H. Xia, F. Yan, M.O. Lai, L. Lu, *J. Funct Mater Lett*, 2 (2009)163.
19. R. Köferstein, *J. Alloys Compd*, 590 (2014) 324.
20. A. Kumar, P. Sharma, W. Yang, J.D. Shen, D. Varshney, *J. Ceramics International.* 42 (2016) 14805–14812.
21. E. Gil-González, A. Perejón, P. E. Sánchez-Jiménez, M.A. Hayward, L.A. Pérez-Maqueda, *J. Journal of the European Ceramic Society*, 37 (2017) 945–954.
22. K.D. Kreuer, *J. Solid-State Ionics*, 97 (1997) 1.
23. G. Deng, Y.G. Chen, M.D. Tao, C.L. Wu, X.Q. Shen, H. Yang, M. Liu, *Electrochim. Acta*, 55 (2010) 884.
24. G. Deng, Y.G. Chen, M.D. Tao, C.L. Wu, X.Q. Shen, H. Yang, M. Liu, *Electrochim. Acta*, 55 (2010) 1120.
25. B.T. Hanga, D.H. Thang, *J. Journal of Alloys and Compounds*, 655 (2016) 44-49.
26. P. Periasamy, B.R. Babu, S.V. Iyer, *J. Power Sources*, 63 (1997) 79-85.
27. R.D. Armstrong, I. Baurhoo, *J. Electroanal. Chem.*, 40 (1972) 325-338.
28. A.J. Salkind, C.J. Venuto, S.U. Falk, *J. Electrochem. Soc.*, 111 (1964) 493-495.
29. L. Ojefors, *J. Electrochem. Soc.*, 123 (1976) 1691-1696.
30. P. Periasamy, B.R. Babu, S.V. Iyer, *J. Power Sources*, 58 (1996) 35-40.
31. M. Song, Y.G. Chen, M.D. Tao, C.L. Wu, D. Zhu, H. Yang, *Electrochim. Acta*, 55 (2010) 3103.
32. B. Singh, C.J. Park, S.J. Song, *Electrochim Acta*,102 (2013) 393.
33. G. Deng, Y.G. Chen, M.D. Tao, C.L. Wu, X.Q. Shen, H. Yang, *Electrochim. Acta*, 54 (2009) 3910.
34. P. Periasamy, B.R. Babu, S.V. Iyer, *J. Power Sources*, 63 (1997) 79.
35. R.D. Armstrong, I. Baurhoo, *Electroanal. Chem*, 40 (1972) 325.
36. A.J. Salkind, C.J. Venuto, S.U. Falk, *J. Electrochem Soc*, 111 (1964) 493.
37. P. Periasamy, B.R.Babu, S.V. Iyer, *J. Power Sources*, 58 (1996) 35.
38. L. Ojefors, *J. Electrochem. Soc*, 123 (1976) 1691.
39. J.F. Sun, Z.P. Li, J.Q. Wang, W. Hong, P.W. Gong, P. Wen, Z.F. Wang, S.R. Yang, *J. Journal of Alloys and Compounds*, 643 (2015) 231–238.
40. F. Li, E.B. Shangguan, J. Li, L.J. Li, J. Yang, Z.R. Chang, Q.M. Li, X.Z. Yuan, H.J. Wang, *Electrochimica. Acta*, 178 (2015) 34–44.
41. B. Liao, Y.Q. Lei, L.X. Chen, *J. Power Source*, 129 (2004) 358.
42. T. Kohno, H.Yoshida, F. Kawashima, *J. Alloys Compd*, 311 (2000) L5.
43. M.Y. Song, D. Ahn, I.H. Kwon, S.H. Chough, *J. Electrochem. Soc*, 148 (2001) A1041.
44. H. Yukawa, Y.Takahashi, M. Morinaga, *J. Comput. Mater. Sci.*, 14 (1999) 291.
45. K. Bouzek, I. Rousar, *J. journal of applied electrochemistry*, 27 (1997) 679–684.
46. S. Barışçı, F. Ulu, H. Särkkä, A. Dimoglo, M. Sillanpää, *Int. J. Electrochem. Sci.*, 9 (2014) 3099 – 3117.

47. Z. Macova, K. Bouzek, V.K. Sharma, *J. Appl Electrochem*, 40 (2010) 1019–1028.
48. C.G. Zhao, X.X. Shao, Y.X. Zhang, X.Z. Qian, *J. ACS Appl. Mater. Interfaces*, 8 (2016) 30133−30142.